JACS
JOURNAL OF THE AMERICAN CHEMICAL SOCIETY
pubs.acs.org/JACS
Article

Targeting the APP-Mint2 Protein–Protein Interaction with a Peptide-Based Inhibitor Reduces Amyloid-β Formation

Christian R. O. Bartling,[§] Thomas M. T. Jensen,[§] Shawna M. Henry,[§] Anna L. Colliander, Vita Sereikaite, Marcella Wenzler, Palash Jain, Hans M. Maric, Kasper Harpsøe, Søren W. Pedersen, Louise S. Clemmensen, Linda M. Haugaard-Kedström, David E. Gloriam, Angela Ho, and Kristian Strømgaard*

Cite This: J. Am. Chem. Soc. 2021, 143, 891–901

ABSTRACT: There is an urgent need for novel therapeutic approaches to treat Alzheimer's disease (AD) with the ability to both alleviate the clinical symptoms and halt the progression of the disease. AD is characterized by the accumulation of amyloid-β (Aβ) peptides which are generated through the sequential proteolytic cleavage of the amyloid precursor protein (APP). Previous studies reported that Mint2, a neuronal adaptor protein binding both APP and the γ-secretase complex, affects APP processing and formation of pathogenic Aβ. However, there have been contradicting results concerning whether Mint2 has a facilitative or suppressive effect on Aβ generation. Herein, we deciphered the APP-Mint2 protein–protein interaction (PPI) via extensive probing of both backbone H-bond and side-chain interactions. We also developed a proteolytically stable, high-affinity peptide targeting the APP-Mint2 interaction. We found that both an APP binding-deficient Mint2 variant and a cell-permeable PPI inhibitor significantly reduced $A\beta_{42}$ levels in a neuronal *in vitro* model of AD. Together, these findings demonstrate a facilitative role of Mint2 in Aβ formation, and the combination of genetic and pharmacological approaches suggests that targeting Mint2 is a promising therapeutic strategy to reduce pathogenic Aβ levels.

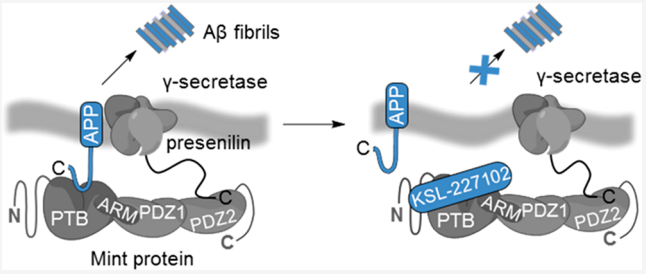

INTRODUCTION

Amyloid-β (Aβ) peptides, the main component of senile amyloid plaques, play a key role in Alzheimer's disease (AD) pathogenesis.[1,2] Aβ peptides are generated by the sequential proteolysis of the amyloid precursor protein (APP),[3] a type I transmembrane protein of 695–770 amino acids. In the pathogenic amyloid cascade, cleavage by an aspartyl protease (BACE-1 or β-secretase) generates a soluble APP ectodomain (sAPPβ) and a membrane-bound C-terminal fragment (C99). Subsequent cleavage of the C99 fragment by γ-secretase generates the APP intracellular domain (AICD) and Aβ fragments of various lengths, including $A\beta_{40}$ and $A\beta_{42}$. The latter exhibits an increased propensity to form insoluble aggregates, which are a hallmark of AD pathology.

The accumulation of Aβ peptides at synaptic sites has detrimental effects on synaptic function, which contributes to the cognitive decline and memory loss associated with AD.[4] The most advanced anti-Aβ drugs in clinical development are anti-Aβ immunotherapies promoting clearance of the Aβ peptide and its aggregates or β-secretase inhibitors intended to interfere with the initial step of Aβ formation.[5] However, both strategies have suffered from failure in late-stage clinical trials,[6,7] and no disease-modifying AD therapy is yet available. Alternative strategies to reduce Aβ formation, such as the modulation of direct binding partners involved in APP trafficking and processing, could therefore increase the chance of developing a successful AD treatment, which is of increasing importance in light of a constantly growing patient population.[8]

Munc18-interacting proteins (Mints, also known as X11s) are a family of adaptor proteins encoded by three distinct genes (*ABPA1*, *ABPA2*, and *ABPA3*) that produce neuron-specific Mint1 (X11α) and Mint2 (X11β) and ubiquitously expressed Mint3 (X11γ).[9−11] Mint proteins consist of a variable isoform-specific N-terminal region and a conserved C-terminal region that contains a phosphotyrosine binding (PTB) domain and two tandem PSD-95/discs large/zonula occludens (PDZ) domains (Figure 1a).[12] The PTB domain of all three Mint proteins binds the conserved endocytic YENPTY motif of APP, which is essential for regulating APP

Received: October 8, 2020
Published: January 5, 2021

https://dx.doi.org/10.1021/jacs.0c10696
J. Am. Chem. Soc. 2021, 143, 891–901

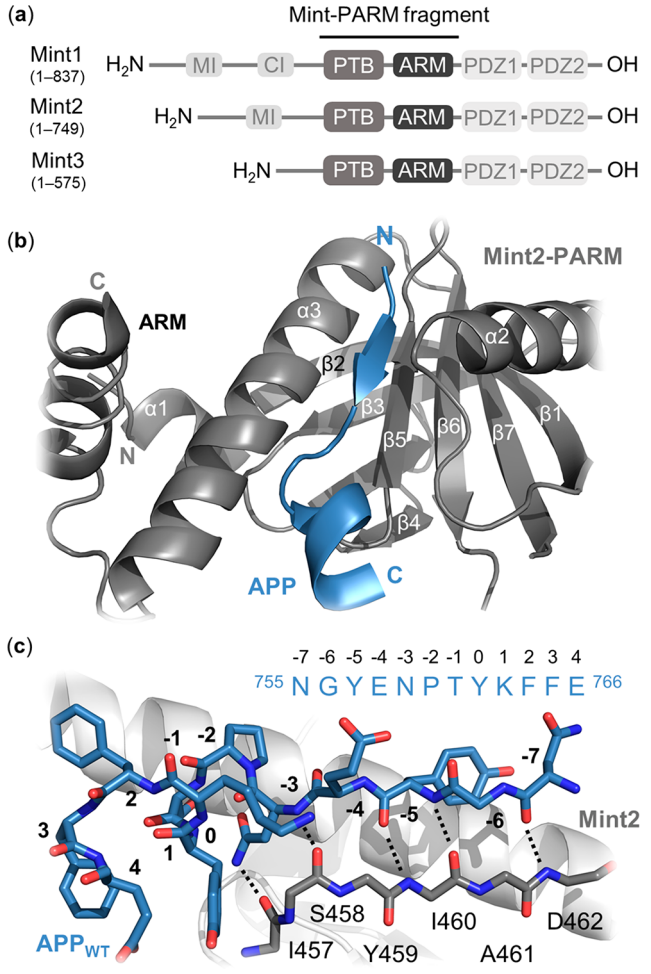

Figure 1. Structural overview of the Mint protein family and the Mint2-APP interaction. (a) Schematic architecture of Mint proteins illustrating their conserved C-terminal region consisting of a phosphotyrosine binding (PTB) domain (gray), an α-helical ARM linker (dark gray), two PSD-95/drosophila discs large/zonula occludens (ZO-1) (PDZ) domains (light gray), and a variable N-terminal region. Numbering corresponds to human residues. MI = Munc-18 interaction domain, CI = CASK interaction domain. (b) Cartoon representation of the interaction between rat Mint2-PARM (gray) and APP (residues 754−767; blue). The $APP_{C\text{-term}}$ is binding at the interface between the α3-helix and β5-strand of Mint2, forming an antiparallel β-sheet (N-terminal) followed by a β-turn and a C-terminal α-helix. The ARM linker (dark gray) is found in an open conformation enabling APP binding. (c) Structure of the APP peptide (blue sticks) bound to the rat Mint2-PTB domain (gray). The β5-strand of the PTB domain (gray stick, side chains not depicted) is shown to highlight the backbone−backbone H-bond network (black dotted lines) between the Mint2-PTB domain and APP (PDB ID: 3SV1).[12]

trafficking and affects Aβ production.[13−16] A number of studies suggest that the APP-Mint protein−protein interaction (PPI) is of particular biological significance in AD. First, the loss of each individual Mint isoform delays age-dependent Aβ plaque formation in mouse models of AD.[17] Second, Mint proteins interact via their PDZ domains with presenilin-1, the catalytic subunit of the γ-secretase complex, thereby promoting APP/presenilin-1 colocalization favoring Aβ formation.[18−21] Third, Mint proteins are found to be upregulated in AD and are reported to associate with neuritic plaques.[22,23] Altogether, these findings indicate that the APP-Mint PPI is of therapeutic relevance to Aβ formation and AD. Efforts have been made to decipher the physiological role of Mint proteins in Aβ formation, and numerous knockout and knockdown studies, using mainly *in vivo* models, have been reported.[17,20,24−30] However, these studies revealed both suppressive and facilitative effects of Mint proteins on Aβ formation. The role of Mint proteins in the formation of pathogenic Aβ remains controversial since no chemical probe perturbing the APP-Mint PPI has been reported.

Herein, we characterized the APP-Mint2 interaction with molecular resolution through extensive substitutional analyses of both the APP C-terminal peptide ligand ($APP_{C\text{-term}}$) and the Mint2 protein. The introduction of backbone amide-to-ester (A-to-E) modifications uncovered an intricate H-bond network at the APP-Mint2 interface, complementing previously published cocrystal structures. Alanine (Ala) substitutions in the PTB domain of Mint2 identified key residues and led to the generation of an APP binding-deficient Mint2 variant that reduced $A\beta_{42}$ generation *in vitro*. Furthermore, we performed a systematic structure−function analysis of the APP C-terminal peptide which facilitated the development of a proteolytically stable macrocyclic peptide exhibiting nanomolar affinity toward Mint2. In a neuronal *in vitro* model of AD, cell-permeable variants of the high-affinity C-terminal APP mimetic peptide demonstrated that modulation of the APP-Mint2 interaction reduces $A\beta_{42}$ levels.

RESULTS AND DISCUSSION

Minimal APP Mint2-PARM Binding Sequence and Semisynthesis of Mint2-PARM Variants. Within the Mint protein family, Mint2 exerts the greatest effect on Aβ formation and was therefore selected as the target protein.[17] The interaction of APP and Mint2 is mediated by the PTB domain of Mint2 and modulated in an autoinhibited open−closed fashion by a C-terminal α-helical linker (termed ARM) adjacent to the PTB domain.[12,31,32] Consequently, we designed a human Mint2-PTB-ARM (Mint2-PARM) construct (PARM-His6; residues 364−570) as a model protein (Figure 1a). To identify the minimal binding sequence of APP, we systematically tested N- and C-terminal truncated variants of the human 17-mer $APP_{C\text{-term}}$ peptide (QNGYENPTYKFFEQMQN; residues 754−770 in APP_{770}). Using a fluorescence polarization (FP) assay (SI section Detailed Methods), we identified a 12-residue-long peptide, designated as the APP_{WT} peptide (NGYENPTYKFFE; residues 755−766; K_i = 4.0 ± 0.2 μM), as the minimal Mint2-PARM binding sequence (Figure S1 and Table S1).

The reported X-ray cocrystal structure of Mint2 and the APP peptide (QNGYENPTYKFFEQ; residues 753−767, Figure 1b, blue) suggests that an intricate network of backbone hydrogen bond (H-bond) interactions and side-chain interactions mediates the APP-Mint2 interaction (Figure 1c, dotted lines).[12,14] Therefore, we probed side-chain interactions by introducing Ala substitutions, whereas backbone H-bond interactions can only be effectively probed by introducing A-to-E substitutions.[33−37] While we generated Mint2-PARM Ala variants through recombinant expression (Table S2), introducing A-to-E substitutions into the Mint2-PARM domain required the development of a semisynthesis strategy. Specifically, we first generated a pseudo-wild-type Mint2-PARM variant (pPARM-His6; residues 364−570; R455K, C483A, C501A, C566A) containing three cysteine (Cys) to Ala substitutions enabling the use of native Ala residues in the

https://dx.doi.org/10.1021/jacs.0c10696
J. Am. Chem. Soc. 2021, 143, 891−901

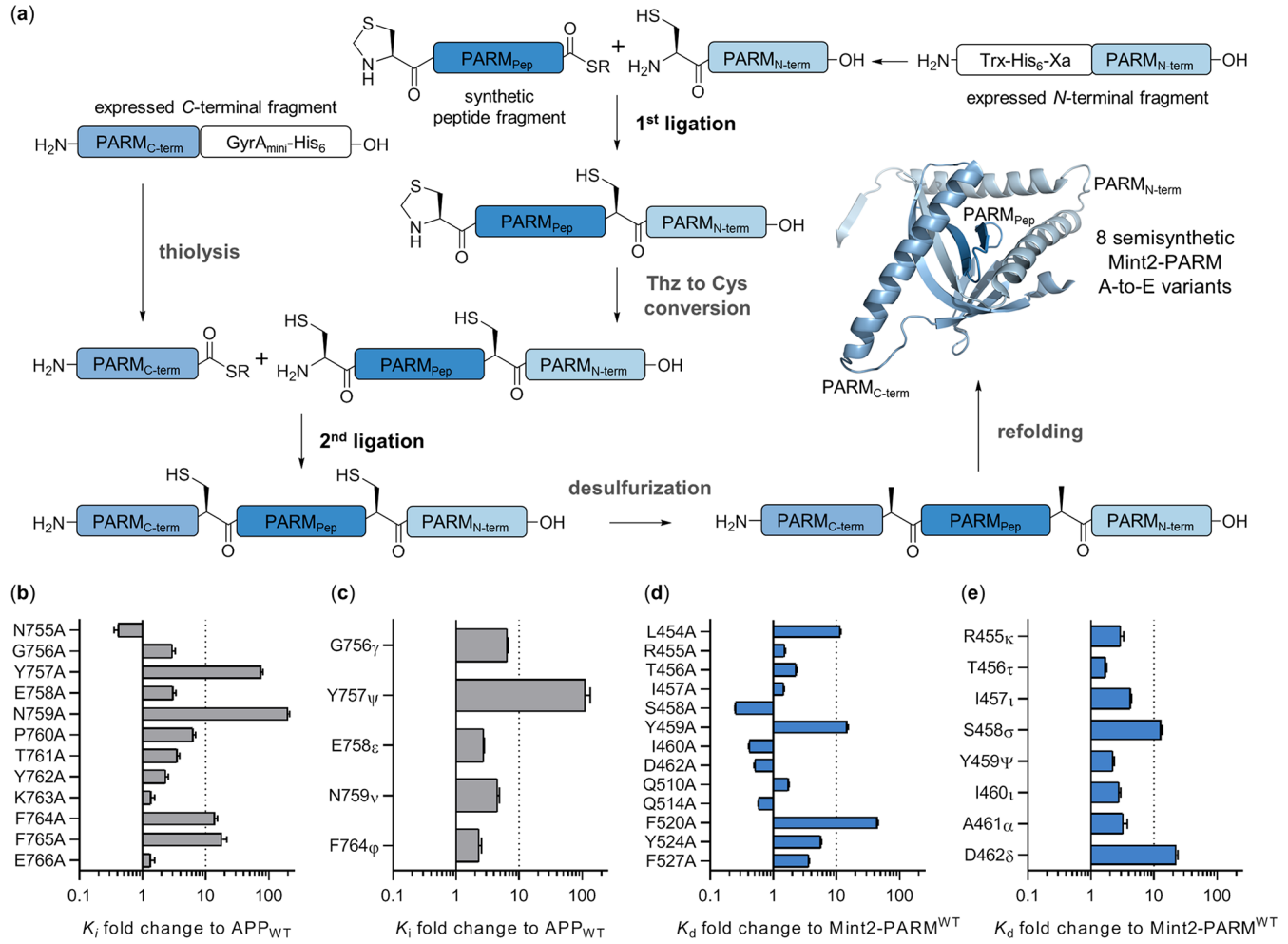

Figure 2. Semisynthesis of Mint2-PARM and effects of A-to-E and Ala mutations in APP and Mint2-PARM. (a) Semisynthetic approach to introducing A-to-E substitutions in Mint2-PARM. N-terminal fragment $PARM_N$ (A479-Q570) is fused to a Xa site to generate an N-terminal Cys by factor Xa cleavage. C-terminal fragment $PARM_C$ (E364-H452) is expressed with a C-terminal intein to generate the required C-terminal thioester. Semisynthesis is initiated by ligating synthetic peptide fragment $PARM_{pep}$ to $PARM_N$. Next, the Thz group is converted to a free Cys and $PARM_{pep+N}$ is ligated to $PARM_C$. Semisynthetic Mint2-pPARM$_{SS}$ is obtained after desulfurization and refolding (Figures S2–S7). (b) Affinity fold-change of the APP_{WT} peptide's Ala-scan and (c) A-to-E substitutions toward Mint2-PARM obtained in an inhibition FP assay (K_i) reported relative to the APP_{WT} peptide [K_i(mutant)/K_i(APP_{WT}) + SEM]. (d) Affinity fold change of the $APP_{C\text{-}term}$ peptide binding to Mint2-PARM Ala and (e) A-to-E variants obtained by the saturation FP assay (K_d) relative to Mint2-PARM^{WT} [K_d(variant)/K_d(wild type) + SEM]. See Figures S8 and S9 for FP data.

native chemical ligation (NCL). Next, we synthesized the same version of Mint2-PARM semisynthetically (pPARM$_{ss}$; residues 364–570; R455K, C483A, C501A, C566A with no His tag) using a three-fragment expressed protein ligation (EPL) approach (Figure 2a). Both protein variants (pPARM-His6 and pPARM$_{ss}$) displayed similar secondary structure and binding affinity for the 17-mer $APP_{C\text{-}term}$ peptide as recombinantly expressed Mint2-PARM (Figures S2 and S3), confirming that neither the His6-tag nor the introduced substitutions affect APP binding. We applied the semisynthetic strategy to introduce eight A-to-E substitutions (R455κ, T456τ, I457ι, S458σ, Y459ψ, I460ι, A461α, and D462δ; α-hydroxy amino acids abbreviated with Greek letters)[38] into Mint2-pPARM$_{SS}$ (Tables S3 and S4), which were all obtained with sufficient yields and purities (Figures S4–S7).

Similarly, we introduced A-to-E substitutions in five positions of the APP_{WT} peptide (G756γ, Y757ψ, E758ε, N759ν, and F764ϕ). The corresponding depsi-peptides were synthesized on the solid phase using α-hydroxy amino acids (SI section Detailed Methods).[39,40] It is generally accepted that A-to-E substitutions do not perturb the overall protein structure.[41] However, the H-bond donor ability of the respective amide-NH is removed and the acceptor capability of the adjacent carbonyl is reduced, which provides a refined tool for studying H-bond networks. A-to-E mutations have successfully been employed to address the significance of backbone H-bonds for folding β-sheet structures and backbone H-bonds in Aβ peptides.[38,42−44]

In total, 21 Mint2-PARM protein variants containing both Ala and A-to-E substitutions and 17 APP_{WT} peptide analogues were generated. We then employed the FP assay to address the consequences of each substitution on the APP-Mint2 interaction (Figure 2b–e).

Backbone H-Bonds and Side-Chain Contacts Are Essential to the APP-Mint2 Interaction. Single-point Ala substitutions in the APP_{WT} peptide resulted in a >10-fold loss of affinity to Mint2-PARM in 4 out of 12 positions (Figure 2b, Figure S8a,b, and Table S1). The substitution of two residues,

https://dx.doi.org/10.1021/jacs.0c10696
J. Am. Chem. Soc. 2021, 143, 891−901

Y757A and N759A located in the endocytic YENPTY motif of APP, resulted in 76-fold and >100-fold decreases in affinity, respectively. In addition, Ala substitution of residues F764 and F765 resulted in 14- and 18-fold decreases in affinity, respectively (Figure 2b). The N-terminal region of the APP peptide forms an antiparallel β-sheet with the β5 strand of Mint2-PARM. On the basis of the X-ray cocrystal structure, H-bond interactions that formed between the APP peptide and Mint2 were probed by A-to-E substitutions (G756γ, Y757ψ, E758ε, and N759ν) (Figure 1c). All four A-to-E substitutions resulted in a reduced binding affinity relative to the APP_{WT} peptide (Figure 2c, Figure S8c,d, and Table S1). Interestingly, the Y757ψ substitution exhibited a >100-fold loss of affinity to Mint2-PARM, as did the Y757A substitution, rendering Y757 as a key residue in APP.

In Mint2-PARM, three Ala substitutions (L454A, Y459A, and F520A) exhibited a >10-fold reduction in the $APP_{C\text{-term}}$ affinity (Figure 2d, Figure S9, and Table S2). The robust effect of Y459A substitution in Mint2-PARM is likely a result of disrupting the hydrophobic interaction with the C_α atom of G756 in APP, an interaction also reported for Mint1 (Y418).[14] Notably, F520A substitution in Mint2-PARM led to a 45-fold reduction in binding affinity, plausibly explained by contacts with key residue N759 in APP (Figure S10a). Corresponding residues in the PTB-domains of Mint1 (F608) and p52 Shc (F198) are also reported to be important for peptide recognition, suggesting that the conserved Phe constitutes an important mediator of ligand recognition for PTB domains.[13,45] Next, we evaluated the effect of A-to-E substitutions in Mint2-PARM on the binding to the $APP_{C\text{-term}}$ peptide. In general, the introduced substitutions reduced the binding affinity of the $APP_{C\text{-term}}$ peptide by 2- to 4-fold (Figure 2e and Table S4). However, two A-to-E substitutions, S458σ and D462δ, resulted in 14- and 25-fold reduced affinities, respectively. Both residues engage in H-bonds and form the antiparallel β-sheet with the N-terminal region of the $APP_{C\text{-term}}$ peptide (Figure 1b,c). Altogether, we identified two key side chains (Y757 and N759) and one backbone amide (Y757ψ) in APP to be critical to the APP-Mint2 interaction. In the Mint2-PTB domain, we found F520A, Y459A, and one backbone amide substitution (D462δ) led to a substantial reduction in affinity to the $APP_{C\text{-term}}$ peptide (Figure 2d, e).

Compared to the reported cocrystal structure of APP and Mint2, we observed a number of deviations from the suggested interactions. First, the side chains of D462 in Mint2 and Y757 in APP are suggested to interact via an H-bond. In our FP measurements, we detected no effect of the D462A mutation in Mint2-PARM on the binding of the $APP_{C\text{-term}}$ peptide (Figure 2d); however, we cannot exclude that the Ala mutation can be compensated for by a water molecule mimicking the H-bond acceptor of D462. Second, Q767 of APP is proposed to H-bond to N387 in Mint2, although the truncated APP_{WT} peptide lacking Q767 retains a wild-type binding affinity (Figure S1). Finally, the side chain of the critical N759 residue in APP is proposed to bind the backbone carbonyls of both L454 and I457 in Mint2.[14] Here, our A-to-E substitutions suggest that only the H-bond protruding from I457 of Mint2 is important, while perturbing the carbonyl of L454 had only minor effects on the affinity to the $APP_{C\text{-term}}$ peptide (Figure 1c).

Mutations in the Mint2-PTB Domain Reduce APP Binding and Aβ Formation. We took advantage of the Mint2-PARM Ala-scan results and designed a Mint2 variant with reduced APP binding affinity. Introducing two mutations, Y459A and F520A, into human Mint2-PARM (hMint2$^{Y459A/F520A}$) resulted in a significant 72-fold decrease in the $APP_{C\text{-term}}$ peptide binding affinity (K_d = 895 ± 43 μM) in the FP assay (Figure 3a and Figure S10). To examine whether

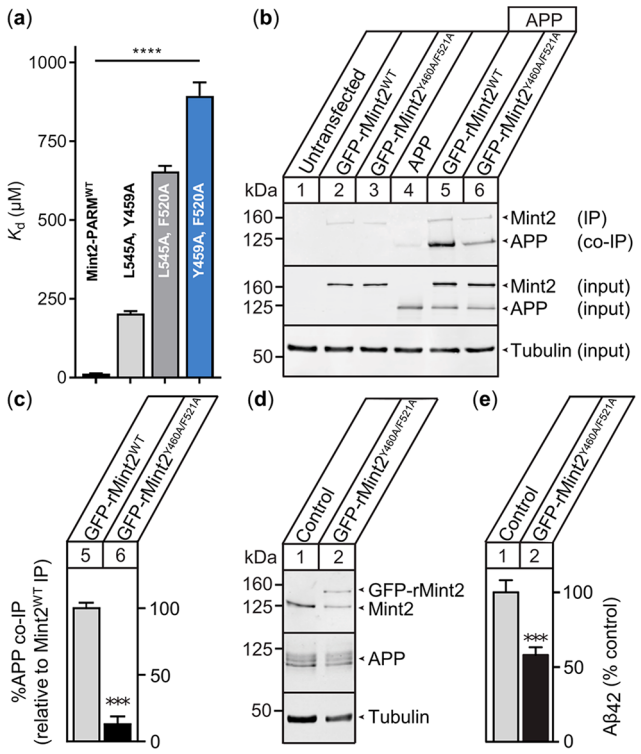

Figure 3. APP binding-deficient rMint2$^{Y460A/F521A}$ variant reduces Aβ_{42} levels in primary mouse neurons. (a) $APP_{C\text{-term}}$ peptide affinity for selected Mint2-PARM variants. Data are expressed as the mean + SEM (n = 3). The statistical significance was evaluated using one-way ANOVA with Dunnett's multiple comparison test, **** P < 0.0001 (Figure S10). (b) Coimmunoprecipitation of APP with the Mint2 antibody from HEK293T cells cotransfected with APP and GFP-rMint2^{WT} or GFP-rMint2$^{Y460A/F521A}$. Western blotting indicates less APP binding to rMint2$^{Y460A/F521A}$ (lane 6) than to GFP-Mint2^{WT} (lane 5). α-Tubulin served as a loading control. (c) Quantification of APP coimmunoprecipitation using GFP-rMint2^{WT} and GFP-rMint2$^{Y460A/F521A}$. Data were normalized to GFP-rMint2^{WT} and expressed as the mean + SEM. The statistical significance was evaluated with the Student's t-test, *** P < 0.001. (n = 4 independent experiments). (d) Western blot for Mint2, APP, and α-tubulin from neuronal lysates carrying the APPswe/PS1ΔE9 mutation and infected with the lentiviral GFP-rMint2$^{Y460A/F521A}$ mutant. (e) Aβ_{42} ELISA quantification of conditioned media from neurons overproducing Aβ shows reduced Aβ_{42} levels when neurons were infected with the GFP-rMint2$^{Y460A/F521A}$ mutant. Data were normalized to the endogenous Mint2^{WT} control and expressed as the mean + SEM (n = 7 biological replicates from two independent experiments). The statistical significance was evaluated using the Student's t-test, *** P < 0.001.

hMint2$^{Y459A/F520A}$ has a cellular effect on APP binding, we produced a full-length GFP-tagged rat Mint2 (GFP-rMint2^{WT}) and corresponding APP binding-deficient variant GFP-rMint2$^{Y460A/F521A}$ (analogous to hMint2$^{Y459A/F520A}$, Figure S11). We confirmed our FP results by cotransfecting HEK293T with full-length APP and either GFP-rMint2^{WT} or GFP-rMint2$^{Y460A/F521A}$ and performing coimmunoprecipitation assays. APP coimmunoprecipitated with both GFP-rMint2^{WT} (lane 5, Figure 3b) and GFP-rMint2$^{Y460A/F521A}$ (lane 6, Figure

https://dx.doi.org/10.1021/jacs.0c10696
J. Am. Chem. Soc. 2021, 143, 891−901

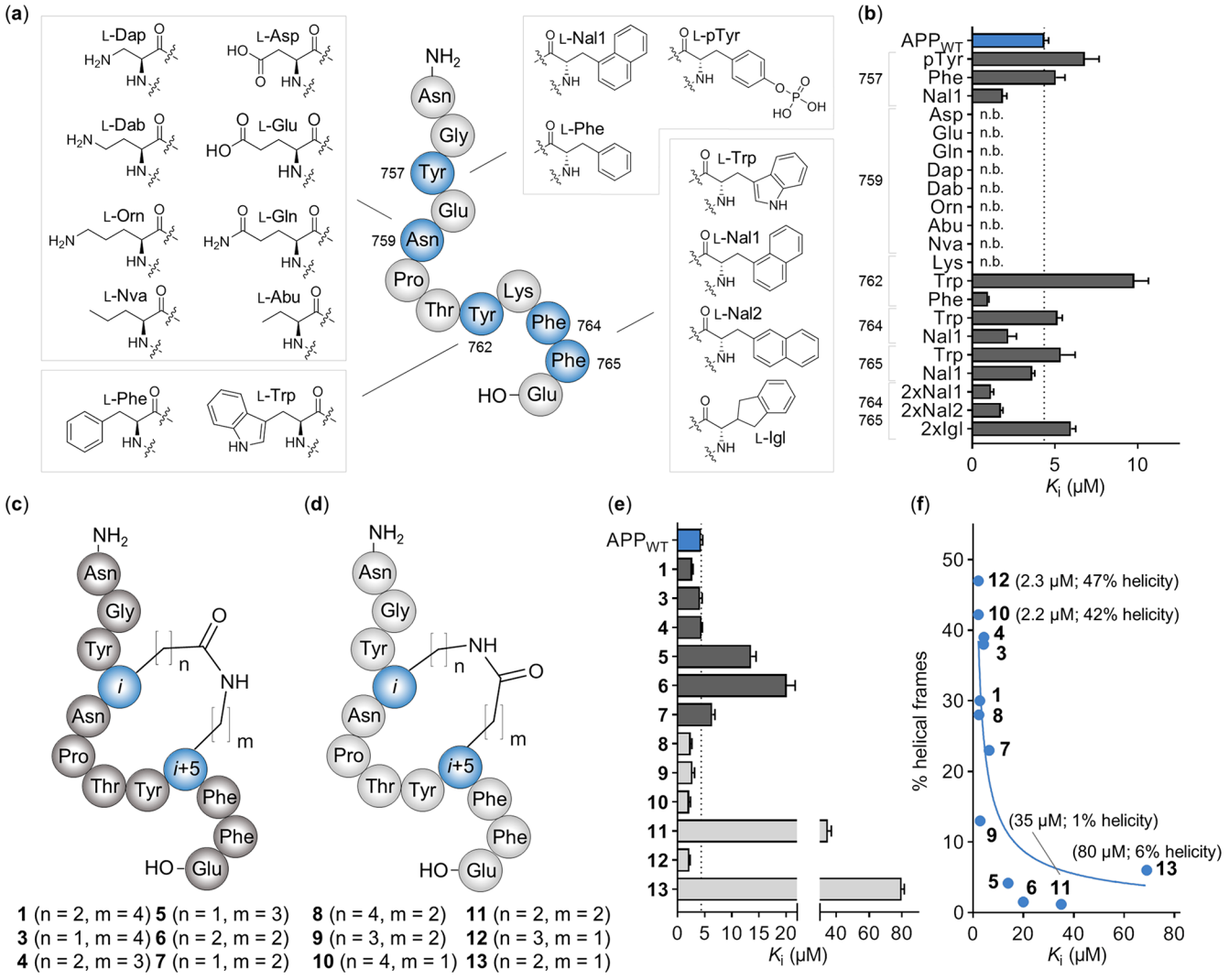

Figure 4. Incorporation of ncAAs and evaluation of side chain-to-side chain macrocyclization in the APP_{WT} peptide. (a) Overview of synthesized APP_{WT} peptide variants, including the structure of the introduced amino acids for each position (blue). (b) K_i values of each APP_{WT} peptide variant measured by FP. n.b. indicates nonbinding peptide (i.e., $K_i \geq 500\ \mu M$). Data are expressed as the mean + SEM ($n = 3$). (c) Structure of side chain-to-side chain cyclized APP_{WT} peptide analogues with native residue order (Glu in the *i* position, dark gray) and (d) inverse residue order (Lys in the *i* position, light gray). (e) K_i values of cyclic APP_{WT} peptide variants measured by FP. Data are expressed as the mean + SEM ($n = 3$). (f) Helical propensity of residues Y762 to E766 from the molecular dynamics simulation of cyclic APP_{WT} peptide variants **1** and **3**−**13** (% helical frames) plotted against the binding affinity (the mean K_i value) including the trend line (blue).

3b); however, GFP-rMint2$^{Y460A/F521A}$ exhibited a significant 85% reduction in APP binding (Figure 3c). Next, we examined the functional effect of an impaired interaction between APP and Mint2 on Aβ generation. We employed primary cortical neurons from an established murine AD model with a double transgene for the expression of mutant APP (APPswe) and presenilin-1 proteins (PS1ΔE9), resulting in enhanced Aβ production.[17] We infected primary neurons with a full-length GFP-rMint2$^{Y460A/F521A}$ lentivirus after 2 days *in vitro* (2 DIV). Expression of the GFP-rMint2$^{Y460A/F521A}$ variant was confirmed by Western blot analysis (Figure 3d). We quantified the effect on Aβ_{42} levels released from primary neurons using an enzyme-like immunosorbent assay (ELISA) on the neuronal conditioned medium. At 15 DIV, we observed a significant 42% decrease in Aβ_{42} levels in neurons infected with GFP-rMint2$^{Y460A/F521A}$ relative to neurons expressing only endogenous Mint2 (Figure 3e). Together, our results confirm that APP interacts with the PTB domain of Mint2 and suggest that Mint2 plays a facilitative role in Aβ formation in our neuronal AD model.

Non-canonical Amino Acids Enhance the Binding of the APP Peptide to Mint2. Since the APP binding-deficient rMint2$^{Y460A/F521A}$ variant reduced Aβ production *in vitro* and previous studies revealed that Mint2 knockout in APPswe/PS1ΔE9 transgenic mice reduces Aβ formation *in vivo*, we hypothesized that a peptide-based inhibitor designed to disrupt the APP-Mint2 interaction could reduce Aβ generation. As such, we used the APP_{WT} peptide as a template for an initial D- and *N*-Me-amino acid (D-AA and *N*Me-AA) scan (Figure S8 and Table S1). D-AAs were tolerated only in the N- and C-termini of the APP_{WT} peptide, whereas the *N*-methylation of N755 resulted in an improved affinity toward Mint2-PARM. Notably, the substitution of Y757 with *N*-MeY757 resulted in a nonbinding APP_{WT} peptide analogue, which is in agreement with the reduced binding of the Y757ψ analogue (Figure 2c). Next, we prepared a series of APP_{WT} peptide variants

https://dx.doi.org/10.1021/jacs.0c10696
J. Am. Chem. Soc. 2021, 143, 891−901

containing single substitutions of both canonical (cAAs) and noncanonical amino acids (ncAAs) (Figure 4a). First, we tested position N759, the most critical residue according to the Ala scan, and introduced eight different amino acids. Remarkably, all substitutions, even conservative ones such as N759Q, abrogated the binding to Mint2-PARM ($K_i \geq 500$ μM) (Figure 4b). We therefore consider N759 to be a key residue in the APP-Mint2 interaction, which is further supported by its conservation as part of the APP endocytic NPXY consensus sequence that interacts with the PTB domain of Mint proteins.[46] Next, we probed the two aromatic residues, F764 and F765. Individual substitution by Trp had no effect on the affinity. In contrast, the incorporation of L-3-(1-naphtyl)alanine (Nal1) at either position improved the affinity for both variants, and the corresponding double substitution showed a 4-fold improvement in affinity ($K_i = 1.1 \pm 0.3$ μM). We attribute the improved affinity to hydrophobic interactions with Y524 and F527 in Mint2-PTB located in close proximity to F764 and F765. Neither L-3-(2-naphtyl)alanine (Nal2) nor 2-indanyl-L-glycine (Igl) improved the affinity to the same extent (Figure 4b).

Finally, the substitution of Y762 to Phe resulted in a 4-fold increase in affinity ($K_i = 1.0 \pm 0.1$ μM), while an Y762W substitution lowered the affinity to Mint2-PARM (Figure 4b and Table S1).

Taken together, we identified six positions (N755, Y757, Y762, F764, F765, and E766) in the APP_{WT} peptide at which substitutions to cAAs or ncAAs either improved the affinity or were expected to improve the proteolytic stability of the peptide.

Side Chain-to-Side Chain Cyclization in the APP_{WT} Peptide Improves Affinity and Stability. To improve the binding and metabolic stability of our peptide ligand, we introduced side chain-to-side chain lactam cyclizations employing solid-phase peptide synthesis (SPPS) and on-resin cyclization (Figure S12a). According to the reported X-ray cocrystal structure of APP-Mint2, native residues E758 and K763 are in close proximity when forming an intramolecular noncovalent salt bridge (Figure S12b).[12] We reasoned that introducing a lactam bridge in this position could confer conformational constraint and potentially improve the affinity and stability.[47] Indeed, a cyclic analogue of the APP_{WT} peptide containing a lactam linkage between E758 and K763 (i to $i + 5$, $cAPP_{E758-K763}$; **1**) exhibited improved affinity compared to the APP_{WT} peptide and was also superior to a variant cyclized between Y762K and E766 (i to $i + 4$, $cAPP_{Y762-E766}$; **2**) (Figure S12b–d). Next, we prepared a series of cyclic variants of **1** in which we systematically modified the lactam bridge by introducing Asp, Orn, or Dap and reversed the orientation of the amide bond in the lactam bridge (Figure 4c,d). The affinity of these 11 peptides (**3**–**13**) was highly dependent on the nature of the introduced macrocyclization (Figure 4e).

In general, macrocyclic peptides with carboxylic acid side chains in i positions (**1** and **3**–**7**; Figure 4c) were characterized by reduced binding affinities, while peptides with amino side chains in i positions (**8**–**13**, Figure 4d) displayed improved affinities relative to the linear APP_{WT} peptide. Furthermore, smaller ring sizes (**5**–**7**, **11**, and **13**) resulted in reduced binding affinities with only peptide **12** ($n = 3$, $m = 1$) refuting this trend. Among the 12 macrocycles, peptide **10** ($n = 4$, $m = 1$) exhibited the highest affinity ($K_i = 2.2 \pm 0.3$ μM) (Figure 4e). To test whether macrocyclization improved the proteolytic stability, cyclic peptide **1** was tested in an *in vitro* human plasma stability assay, resulting in a 4-fold-improved half-life time ($T_{1/2}$) over the APP_{WT} peptide, $T_{1/2} = 105$ and 26 min, respectively (Figure S12e).[48]

On one hand, the moderately improved affinity might be a result of the introduced constrain causing a preorganization of the peptide resembling the bound conformation with a well-defined helical turn of residues Y762–E766, which reduces the entropic penalty upon binding. On the other hand, additional favorable interactions by the formed lactam bridge can also account for the improved affinity. We performed molecular dynamics (MD) simulations of cyclized peptides **1** and **3**–**12** and found a correlation between the degree of helicity in solution and the observed binding affinities. For the two most potent cyclic peptides **10** and **12**, helical propensity predictions of 42 and 47%, respectively, were observed. In contrast, for low-affinity peptides **11** and **13** the molecular dynamics simulations suggested helical propensities of 6% and less (Figure 4f). This suggests that ligand preorganization is the driving force of the improved binding. Altogether, the systematic lactam macrocyclization scan led to the identification of a cyclic APP_{WT} peptide scaffold with improved binding affinity and proteolytic stability.

Identification of a Metabolically Stable, High-Affinity Mint2 Inhibitor Derived from the APP_{WT} Peptide. To develop a potent and proteolytically stable modulator of the APP-Mint2 PPI, we selected cyclic peptide **10** ($n = 4$, $m = 1$) as a scaffold. Next, we introduced D-*N*-Me-Ala and D-Glu at positions 755 and 766, respectively. Finally, ncAA L-Nal1 was selected for positions 764 and 765. The corresponding peptide, KSL-221036 (*N*Me-aGY*cyclo*-[KNPTYD]Nal1Nal1e-OH, **14**), was generated through SPPS including on-resin cyclization via orthogonally protected Lys(Aloc) and Asp(All) (Figure 5a). We found that **14** binds Mint2-PARM with nanomolar affinity ($K_d = 53 \pm 2$ nM) as determined by isothermal titration calorimetry (ITC). Compared to the APP_{WT} peptide ($K_d = 2.4$ μM), a 46-fold improved affinity was achieved (Figure 5b and Figure S13). Furthermore, **14** was found to be proteolytically stable over 24 h (half-life $\geq$ 1440 min) in human plasma (Figure 5c), while the APP_{WT} peptide exhibited a half-life of <30 min. Finally, we examined the rate of metabolism through cytochrome P450 enzymes using mouse liver microsomes and determined the *in vitro* hepatic clearance of the APP_{WT} peptide and **14**. We found the APP_{WT} peptide was cleared fast [$CL_{(int)} = 15.4 \pm 2.5$ μL/(mg min)] while **14** was not metabolized over 60 min [$CL_{(int)} = 0.0 \pm 0.8$ μL/(mg min)] (Figure 5d). This data demonstrates the design of a peptide using the minimal binding sequence of the endogenous APP peptide–ligand as a template. Macrocyclization and the incorporation of selected ncAAs resulted in the design of KSL-221036 (**14**), the first reported modulator of the APP-Mint2 PPI exhibiting nanomolar affinity and suitable stability characteristics for further studies.

KSL-221036 (14) Interacts with Mint2 and Reduces Aβ Levels. To determine whether KSL-221036 (**14**) binds full-length Mint2 from primary neuronal lysate, we loaded the APP_{WT} peptide and **14** onto epoxy-coated magnetic beads via an N-terminal Cys-PEG linker (Table S1). Pull-down from the lysate of primary mouse neurons confirmed that **14** efficiently interacts with endogenous Mint2 at higher affinity (lane 2, Figure 5e) than for the APP_{WT} peptide under the same conditions (lane 3, Figure 5e; see also Figure S14).

To examine the effect of **14** on $A\beta_{42}$ production in neurons, we attached cell-penetrating peptide (CPP) TAT^{47-57} (YGR-

https://dx.doi.org/10.1021/jacs.0c10696
J. Am. Chem. Soc. 2021, 143, 891–901

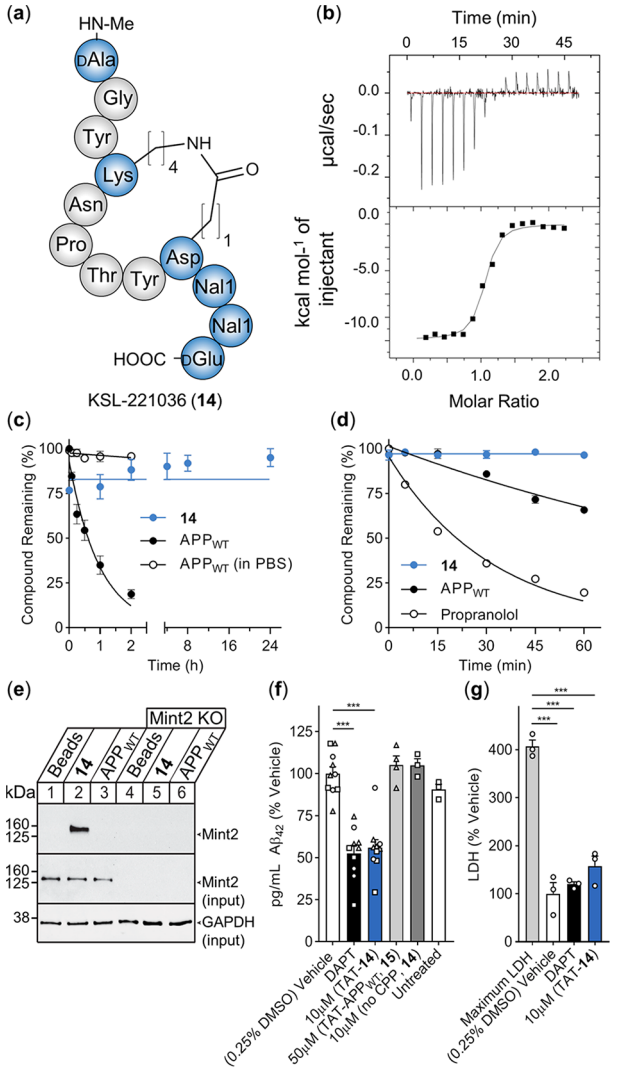

Figure 5. PPI inhibitor of the APP-Mint2 interaction reduces Aβ_{42} production in the neuronal *in vitro* model of AD. (a) Schematic structure of KSL-221036 (**14**). (b) Representative ITC of titrating Mint2-PARM with **14**; raw heat signature (top) and integrated molar heat release (bottom). (c) *In vitro* plasma stability of **14** (blue) and the APP$_{WT}$ peptide (black) including buffer control for the APP$_{WT}$ peptide (circles); data are expressed as the mean ± SEM (n = 3). (d) *In vitro* hepatic clearance of **14** (blue) and the APP$_{WT}$ peptide (black) including propranolol control (circles, n = 1); data are expressed as the mean ± SEM (n = 3). (e) Representative pull down of Mint2 from neuronal cell lysate (15 DIV). Lanes 1−3: expression of Mint2. Lanes 4−6: knockout of Mint2. The eluent was resolved by SDS-PAGE and immunoblotted for Mint2 and GAPDH (n = 3). (f) Aβ_{42} ELISA quantification from conditioned media of neurons over-producing Aβ; data are normalized to the vehicle control and expressed as the mean + SEM (n = 3 independent experiments, n = 10 biological replicates for the vehicle, DAPT, and TAT-**14** (10 μM). Independent experiments are represented by different shapes. Statistical significance evaluated using one-way ANOVA with Dunnett's multiple comparison test, ***P < 0.001. (g) LDH levels from conditioned medium of cultured neurons overproducing Aβ collected after 24 h of treatment with DAPT and TAT-**14** (10 μM). Maximum LDH represents the maximum amount of LDH released from neurons lysed using detergent. Individual data points in (g) correspond to data in panel (f) (circles = same assay). Data are expressed as %LDH normalized to vehicle control and shown as the mean + SEM. Statistical significance was evaluated using one-way ANOVA with Sidak's multiple comparison test, ***P < 0.001.

KKRRQRRR)[49] to the N-terminus of **14** (TAT-**14**) and the APP$_{WT}$ peptide (**15**, Table S1). TAT is a widely used CPP and was recently demonstrated to be compatible with late-stage clinical development in two phase III clinical trials (ESCAPE[50] and FRONTIER), rendering TAT the most advanced CPP tag in the clinic. We first treated neurons with a concentration curve of peptide TAT-**14** to determine the highest concentration at which no adverse effect on cell viability was observed. Using primary neurons and a colorimetric readout of metabolic activity, peptides **14** (no CPP) and **15** (TAT-APP$_{WT}$) exhibited no adverse effect while peptide TAT-**14** affected cell viability at 20 μM (75%) but had no measurable effect at 10 μM (Figure S15). To determine whether modulation of the APP-Mint2 interaction affects Aβ production, primary cortical neurons (14 DIV) carrying a double transgene for the expression of mutant APP (APPswe) and presenilin-1 proteins (PS1ΔE9) were incubated for 24 h with peptides **14**, TAT-**14**, and **15**. ELISA quantification of Aβ_{42} from the conditioned medium revealed that TAT-**14** (10 μM) led to a 44% reduction of Aβ_{42} levels relative to vehicle control. In contrast, TAT-APP$_{WT}$ (**15**, 50 μM) and **14** (10 μM, no CPP) did not affect Aβ_{42} levels. High-affinity γ-secretase inhibitor DAPT (*N*-[*N*-(3,5-difluorophenacetyl)-L-alanyl]-S-phenyl-glycine *tert*-butyl ester or LY-374973) served as a positive control, reducing Aβ_{42} levels by 47% (Figure 5f and Figure S16).[51] In addition, we assessed the effect of TAT-**14** on cellular integrity by quantifying lactate dehydrogenase (LDH) release (a proxy for cytotoxicity) in the same conditioned medium used for the aforementioned ELISA. We found low LDH levels for both DAPT- and TAT-**14**-treated neurons relative to vehicle control, indicating that the effect of peptide TAT-**14** on Aβ production is not due to cellular toxicity (Figure 5g; see also Figure S16). Furthermore, p-value analysis found no significant difference between the vehicle and TAT-**14** (p = 0.2448) or DAPT and TAT-**14** (p = 0.6525) LDH release. To further support the TAT-mediated intracellular delivery of **14**, we detected TAT immunostaining in primary neurons incubated with TAT-**14** (Figure S17), indicating that TAT-**14** is cell-permeable.

Following the promising Aβ_{42} results of TAT-**14**, we investigated the dose−response relationship and found a weak correlation between the concentration of TAT-**14** and reduced Aβ_{42} levels (Figure S16e). We reasoned that the delivery efficiency of the cargo potentially depends on the employed CPP tag; therefore, we synthesized four additional variants of **14** containing different CPPs attached to the N-terminus: mixTAT-**14** (rRrGrKkrK-**14**), polyArg-**14** (RRRRRRRRR-**14**),[52] D-SynB3-**14** (frrrsyslrr-**14**),[53] and Mini-Ap4-**14** (*cyclo*(DLATEPAK(Dap)-**14**).[54] Next, we determined the highest concentration at which no adverse effect on cell viability was observed. Peptide MiniAp4-**14** exhibited no toxicity, while peptides mixTAT-**14** and polyArg-**14** were tolerated at concentrations of 5 and 7.5 μM, respectively (Figure S15). Peptide D-SynB3-**14** was poorly soluble and not further tested. The peptides' effect on Aβ formation was evaluated analogously to that of peptide TAT-**14**. The quantification of Aβ_{42} from the conditioned medium of primary neurons revealed that incubation with mixTAT-**14** (5 μM) and polyArg-**14** (5 μM) reduced Aβ_{42} levels by 80 and 84%, respectively. In contrast, incubation with MiniAp4-**14** (10 μM) did not affect Aβ_{42} production (Figure S16c). Of note, we detected a small increase in LDH activity following incubation with mixTAT-**14** (5 μM) compared to the vehicle control

https://dx.doi.org/10.1021/jacs.0c10696
J. Am. Chem. Soc. 2021, 143, 891−901

(Figure S16d). Consequently, polyArg-**14**, which reduced Aβ_{42} production at a lower concentration (5 μM) with minimal cellular toxicity, is a promising CPP alternative to TAT-**14**.

Our results indicate that peptide **14** successfully binds Mint2 *in vitro* with greater affinity than the APP$_{WT}$ peptide. Further studies in primary neurons cultured from our AD mouse model revealed that TAT-**14** significantly decreases Aβ_{42} production with minimal toxicity. Further investigation into alternative CPPs showed that polyArg also provides attractive properties that facilitate the cellular uptake of peptide ligand **14**. The observation that TAT-APP$_{WT}$ (**15**) has no effect on Aβ_{42} formation is in excellent agreement with the pull-down results and highlights the importance of ligand optimization. According to the reported effects of Mint knockout on APP trafficking and Aβ_{42} formation,[21] inhibition of the Mint2-APP PPI by compounds TAT-**14** and polyArg-**14** could either result in reduced APP endocytosis or prevent the formation of the tertiary protein complex comprising APP (C99), Mint2, and the γ-secretase. Both avenues ultimately result in reduced Aβ formation. As such, the lowered Aβ_{42} levels seen in the *in vitro* AD model following treatment with compounds TAT-**14** and polyArg-**14** provide evidence that modulation of the APP-Mint2 PPI might serve as a pharmacological strategy to reduce pathologic Aβ levels in connection with AD.

CONCLUSIONS

In the pursuit of novel strategies to treat AD, pharmacological approaches modulating direct binding partners involved in APP trafficking and processing are promising alternatives to currently pursued therapies. Here, the APP-Mint PPI is an attractive target as the effects of Mint deletions are relatively mild, and our strategy, which selectively inhibits APP binding to the PTB domain of Mint proteins, would likely not interfere with the critical function of Mint proteins in synaptic vesicle exocytosis,[17] which is mediated through Mint's other PPI domains.[9] Although numerous studies have examined the biological importance of Mint proteins, particularly with regard to Aβ formation in the context of AD,[30] these studies have been informative but contradictory.[55]

Here, we extensively characterized the APP-Mint2 interaction at the molecular level by performing comprehensive mutational scans of the APP-Mint2 interface, covering both side-chain and backbone interactions. Compared to the reported structures, we observed distinct differences and showed that two backbone alterations, Y757ψ in the APP$_{WT}$ peptide and D462δ in Mint2, had major impacts on the APP-Mint2 interaction. The introduction of Ala substitutions demonstrated that the side chains of two residues in APP, N759, and Y757 and one residue in Mint2, F520, are pivotal to the APP-Mint2 interaction. These observations led to the generation of a Mint2 variant containing two distinct substitutions, Y459A/F520A, which resulted in impaired APP binding. We showed that reduced APP binding results in significantly reduced Aβ production, which supports a facilitative role of Mint2 in Aβ formation and suggests that targeting the APP-Mint2 interaction with a PPI inhibitor is of potential therapeutic relevance.

Using the APP$_{WT}$ peptide as a template, we developed a high-affinity, proteolytically stable cyclic peptide **14**. We demonstrated that introducing noncanonical amino acids, N-methylation, and D-amino acids into a macrocyclic peptide scaffold provided a vast improvement in affinity for Mint2 and stability relative to the APP$_{WT}$ peptide. Notably, compared to APP$_{WT}$, peptide **14** exhibited an enhanced affinity to robustly pull down full-length Mint2 from neuronal lysate. We confirmed that targeting the Mint2-APP interaction with cell-permeable variants of **14** (TAT-**14** and polyArg-**14**) significantly reduced Aβ_{42} formation, whereas parent APP$_{WT}$ peptide **15** had no effect on Aβ_{42} formation. Peptides TAT-**14**, mixTAT-**14**, and polyArg-**14** therefore provide first proof-of-concept evidence that targeting a direct interaction partner of APP affects its metabolism and Aβ formation. Furthermore, the comparison of different CPP tags indicates that the selection is critical and affects not only efficacy but also neuronal viability. Here, the combined analysis of LDH levels and Aβ_{42} reduction suggests that polyArg-**14** might be preferred over TAT-**14** (Figure S16).

Previous work has shown that APP and BACE-1 converge in acidic microdomains.[56,57] Because the BACE-1 cleavage of APP is the rate-limiting step in Aβ production,[58] this convergence in endosomes is a critical initiator of the APP amyloidogenic cascade. Sullivan et al. reported that the knockout of Mint proteins resulted in reduced APP endocytosis and Aβ formation.[21] We suspect that the APP binding-deficient rMint2$^{Y460A/F521A}$ variant and TAT-, mix-TAT-, and polyArg-**14** could have a similar effect. The same study reported that the knockout of Mint proteins also affects the internalization of presenilin-1 of the γ-secretase complex and reduced colocalization with APP.

The impaired binding of APP (C99 fragment) to Mint2 and presenilin-1 would reduce the probability of γ-site cleavage in APP and hence Aβ formation. Our results encompass both observations.

In summary, we demonstrated that targeting the APP-Mint PPI may present an alternative strategy in the pursuit of new therapeutic approaches in AD treatment. We believe that the compounds reported herein will be of help in identifying mechanisms of Mint2-mediated Aβ formation and enable future *in vivo* studies.

METHODS

Detailed experimental procedures are provided in the Supporting Information.

Peptide Synthesis. Peptides and depsipeptides were assembled in a manual or automated manner (LibertyBlue, CEM, Matthews, NC, USA) on a solid support using Boc- or Fmoc-based chemistry, purified by RP-HPLC, and characterized by LCMS and UPLC. When relevant, side-chain cyclization was performed on resin by the deprotection of Alloc and Allyl protecting groups, followed by PyBOP-induced cyclization.

Protein Expression. Human Mint2 constructs were cloned in pRSET, pET, or pTXB1 vectors, expressed in *E. coli* Bl21(DE3)pLysS (Invitrogen), and purified using HisTrap columns, followed by size-exclusion chromatography on a HiLoad 16/600 Superdex 75 pg column or purification by reverse-phase chromatography (C4 column, YMC-Pack-C4, 250 × 20 mm^2).

Expressed Protein Ligation. The three-step ligation was initiated by ligating PARM$_N$ to the thioester peptide (PARM$_{Pep}$) fragment. Following buffer exchange, the second ligation was performed using the PARM$_C$ fragment. Obtained proteins were purified using a reverse-phase C4 column (Jupitor, Phenomenex, 250 × 10 mm^2). After desulfurization, the semisynthetic protein was refolded into storage buffer and characterized by LCMS and UPLC.

Circular Dichroism (CD). Experiments were performed on an Olis DSM 100 (Olis Inc.) at 15 μM protein concentration, and the obtained millidegrees of ellipticity (mo) was converted to the mean residue ellipticity (θ_{MRE}).

https://dx.doi.org/10.1021/jacs.0c10696
J. Am. Chem. Soc. 2021, 143, 891−901

ThermoFluor. ThermoFluor experiments were performed in a 96-well plate format on a Stratagene Mx3005p qPCR cycler (Agilent) using SYPRO orange as the dye at 15 μM protein concentration.

Fluorescent Polarization (FP). Saturation binding (for semi-synthetic and mutated proteins) using 50 nM TAMRA-APP$_{C\text{-term}}$ [(TAMRA)-NNG-QNGYENPTYKFFEQMQN] as a probe was performed using a Safire2 plate reader (Tecan) and increasing concentrations of Mint2-PARM. Inhibition experiments were performed using 50 nM TAMRA-APP$_{C\text{-term}}$ and 15 μM Mint2-PARM at increasing concentrations of peptide ligands.

Rat Mint2$^{Y460A/F521A}$ Cloning. Using a QuikChange II Site-Directed Mutagenesis Kit (Agilent Technologies), pEGFP-rMint2$^{Y460A/F521A}$ was created from rat pEGFP-Mint2 and subcloned into the lentiviral pFUW vector for neuronal expression.

HEK293T Coimmunoprecipitation. Transfected HEK293T cells were lysed, and protein extracts were incubated with precipitating antibody and protein A Ultralink resin (Thermo Scientific). Precipitated proteins were resolved by SDS-PAGE and immunoblotted for APP, GFP, and α-tubulin.

Primary Neuron Infection with rMint2$^{Y460A/F521A}$ and Aβ ELISA. Primary neuronal cultures were prepared from newborn mice and infected with lentivirus for rMint2$^{Y460A/F521A}$. At 15 DIV, neuronal lysate was collected, resolved by SDS-PAGE, and immunoblotted for APP, Mint2, and α-tubulin. Conditioned media were collected and handled according to a Human Aβ_{42} Ultrasensitive ELISA Kit (Invitrogen).

Molecular Dynamics Simulations. The Desmond package in Schrodinger's Maestro suite was used to perform molecular dynamics simulations. Each simulation was run in duplicate (200 ns) under standard temperature and pressure. The simulation output was parsed frame by frame using Python, and helical propensity values were determined.

***In vitro* Plasma Stability.** Peptides were incubated in human plasma at 37 °C for up to 24 h. The peptides were extracted from the plasma at various time points and analyzed using UPLC.

***In vitro* Hepatic Clearance.** Peptides were incubated in mouse hepatic microsomes supplemented with reduced β-nicotinamide adenine dinucleotide 2′-phosphate (NADPH) and $MgCl_2$ at 37 °C for up to 60 min. The peptides were extracted from the microsomes at various time points and analyzed using UPLC.

Isothermal Titration Calorimetry (ITC). Experiments were performed using an ITC200 (Malvern). Ligand-to-buffer titrations were performed to subtract the heat produced by injection, mixing, and dilution. The binding enthalpy was directly measured, and the dissociation constant (K_d) and stoichiometry (N) were obtained by data analysis using Origin software (OriginLab).

Neuronal Cell Viability. Primary neuron cultures were treated with peptides or DMSO as indicated. The cell viability and cytotoxicity were determined using a CellTiter 96 AQ$_{ueous}$One Solution Cell Proliferation Assay (MTS) Kit (Promega) and a CyQUANT LDH Cytotoxicity Assay (Thermo Fisher).

Immobilization of Peptides. Peptide KSL-221036 and the APP$_{WT}$ peptide comprising a C-terminal Cys and a PEG2 linker were loaded onto Dynabeads M-270 Epoxy Beads (Thermo Fischer Scientific) according to the protocol of the manufacturer.

Protein Isolation from Neuronal Cell Lysate. Primary neuronal cultures were prepared as described above. Neurons expressing Mint2 were infected with lentiviral inactive *cre* recombinase, while Mint2 knockout neurons were infected with active *cre* recombinase. At DIV15, neuronal lysate was collected and incubated with peptide-loaded Dynabeads. Isolated proteins were resolved by SDS-PAGE and immunoblotted for Mint2 and GAPDH.

ELISA Aβ Assay Following Peptide Treatment. Primary neuronal cultures were prepared from newborn transgenic mice carrying the APPswe/PS1$\Delta E9$ transgene. At 15 DIV, neurons were incubated with peptides, DAPT (γ-secretase inhibitor), and vehicle control 0.25% DMSO. The collected conditioned media were handled according to the protocol of the Human Aβ_{42} Ultrasensitive ELISA Kit (Invitrogen).

Data Analysis. All data analysis was performed in GraphPad Prism 7.0 (GraphPad Inc.), Excel 2010 (Microsoft), and Origin 9.0 (OriginLab). Significance was evaluated using the Student's t test in the case of two groups. The one-way ANOVA test was used in the case of three or more groups, combined with either Dunnett's or Sidak's multiple comparison test.

■ ASSOCIATED CONTENT

Supporting Information

The Supporting Information is available free of charge at https://pubs.acs.org/doi/10.1021/jacs.0c10696.

Synthesis and additional experimental and analytical details (PDF).

■ AUTHOR INFORMATION

Corresponding Author

Kristian Strømgaard − *Department of Drug Design and Pharmacology, University of Copenhagen, DK-2100 Copenhagen, Denmark;* orcid.org/0000-0003-2206-4737; Email: kristian.stromgaard@sund.ku.dk

Authors

Christian R. O. Bartling − *Department of Drug Design and Pharmacology, University of Copenhagen, DK-2100 Copenhagen, Denmark; Department of Biology, Boston University, Boston, Massachusetts 02215, United States*

Thomas M. T. Jensen − *Department of Drug Design and Pharmacology, University of Copenhagen, DK-2100 Copenhagen, Denmark*

Shawna M. Henry − *Department of Biology, Boston University, Boston, Massachusetts 02215, United States*

Anna L. Colliander − *Department of Drug Design and Pharmacology, University of Copenhagen, DK-2100 Copenhagen, Denmark*

Vita Sereikaite − *Department of Drug Design and Pharmacology, University of Copenhagen, DK-2100 Copenhagen, Denmark*

Marcella Wenzler − *Department of Drug Design and Pharmacology, University of Copenhagen, DK-2100 Copenhagen, Denmark*

Palash Jain − *Department of Drug Design and Pharmacology, University of Copenhagen, DK-2100 Copenhagen, Denmark*

Hans M. Maric − *Department of Drug Design and Pharmacology, University of Copenhagen, DK-2100 Copenhagen, Denmark*

Kasper Harpsøe − *Department of Drug Design and Pharmacology, University of Copenhagen, DK-2100 Copenhagen, Denmark;* orcid.org/0000-0002-9326-9644

Søren W. Pedersen − *Department of Drug Design and Pharmacology, University of Copenhagen, DK-2100 Copenhagen, Denmark*

Louise S. Clemmensen − *Department of Drug Design and Pharmacology, University of Copenhagen, DK-2100 Copenhagen, Denmark*

Linda M. Haugaard-Kedström − *Department of Drug Design and Pharmacology, University of Copenhagen, DK-2100 Copenhagen, Denmark*

David E. Gloriam − *Department of Drug Design and Pharmacology, University of Copenhagen, DK-2100 Copenhagen, Denmark*

Angela Ho − *Department of Biology, Boston University, Boston, Massachusetts 02215, United States*

Complete contact information is available at:

https://dx.doi.org/10.1021/jacs.0c10696
J. Am. Chem. Soc. 2021, 143, 891−901

https://pubs.acs.org/10.1021/jacs.0c10696

Author Contributions

§C.R.O.B., T.M.T.J., and S.M.H. contributed equally.

Notes

The authors declare no competing financial interest.

■ ACKNOWLEDGMENTS

We thank the Lundbeck Foundation for financial support provided to K.S. and NIH R01 AG044499 for financial support provided to A.H. We also thank Christian A. Olsen, Stephan A. Pless, Mette Ishøy Rosenbaum, and Dennis Özcelik for their critical input.

■ REFERENCES

(1) Wang, J.; Gu, B. J.; Masters, C. L.; Wang, Y. J. A systemic view of Alzheimer disease - insights from amyloid-beta metabolism beyond the brain. *Nat. Rev. Neurol.* **2017**, *13* (10), 612−623.

(2) Selkoe, D. J.; Hardy, J. The amyloid hypothesis of Alzheimer's disease at 25 years. *EMBO Mol. Med.* **2016**, *8* (6), 595−608.

(3) Müller, U. C.; Deller, T.; Korte, M. Not just amyloid: physiological functions of the amyloid precursor protein family. *Nat. Rev. Neurosci.* **2017**, *18* (5), 281−298.

(4) Haass, C.; Selkoe, D. J. Soluble protein oligomers in neurodegeneration: lessons from the Alzheimer's amyloid beta-peptide. *Nat. Rev. Mol. Cell Biol.* **2007**, *8* (2), 101−112.

(5) Panza, F.; Lozupone, M.; Logroscino, G.; Imbimbo, B. P. A critical appraisal of amyloid-beta-targeting therapies for Alzheimer disease. *Nat. Rev. Neurol.* **2019**, *15* (2), 73−88.

(6) Hawkes, N. Merck ends trial of potential Alzheimer's drug verubecestat. *BMJ.* **2017**, *356*, j845.

(7) Honig, L. S.; Vellas, B.; Woodward, M.; Boada, M.; Bullock, R.; Borrie, M.; Hager, K.; Andreasen, N.; Scarpini, E.; Liu-Seifert, H.; Case, M.; Dean, R. A.; Hake, A.; Sundell, K.; Poole Hoffmann, V.; Carlson, C.; Khanna, R.; Mintun, M.; DeMattos, R.; Selzler, K. J.; Siemers, E. Trial of Solanezumab for Mild Dementia Due to Alzheimer's Disease. *N. Engl. J. Med.* **2018**, *378* (4), 321−330.

(8) Alzheimer's Association. 2017 Alzheimer's disease facts and figures. *Alzheimer's Dementia* **2017**, *13*(4), 325−373.

(9) Okamoto, M.; Sudhof, T. C. Mints, Munc18-interacting proteins in synaptic vesicle exocytosis. *J. Biol. Chem.* **1997**, *272* (50), 31459−31464.

(10) Okamoto, M.; Südhof, T. C. Mint 3: A ubiquitous mint isoform that does not bind to munc18−1 or −2. *Eur. J. Cell Biol.* **1998**, *77* (3), 161−165.

(11) Rogelj, B.; Mitchell, J. C.; Miller, C. C.; McLoughlin, D. M. The X11/Mint family of adaptor proteins. *Brain Res. Rev.* **2006**, *52* (2), 305−315.

(12) Xie, X.; Yan, X.; Wang, Z.; Zhou, H.; Diao, W.; Zhou, W.; Long, J.; Shen, Y. Open-closed motion of Mint2 regulates APP metabolism. *J. Mol. Cell Biol.* **2013**, *5* (1), 48−56.

(13) Borg, J. P.; Ooi, J.; Levy, E.; Margolis, B. The phosphotyrosine interaction domains of X11 and FE65 bind to distinct sites on the YENPTY motif of amyloid precursor protein. *Mol. Cell. Biol.* **1996**, *16* (11), 6229−6241.

(14) Zhang, Z.; Lee, C. H.; Mandiyan, V.; Borg, J. P.; Margolis, B.; Schlessinger, J.; Kuriyan, J. Sequence-specific recognition of the internalization motif of the Alzheimer's amyloid precursor protein by the X11 PTB domain. *EMBO J.* **1997**, *16* (20), 6141−6150.

(15) King, G. D.; Perez, R. G.; Steinhilb, M. L.; Gaut, J. R.; Turner, R. S. X11α modulates secretory and endocytic trafficking and metabolism of amyloid precursor protein: Mutational analysis of the YENPTY sequence. *Neuroscience* **2003**, *120* (1), 143−154.

(16) Ring, S.; Weyer, S. W.; Kilian, S. B.; Waldron, E.; Pietrzik, C. U.; Filippov, M. A.; Herms, J.; Buchholz, C.; Eckman, C. B.; Korte, M.; Wolfer, D. P.; Müller, U. C. The secreted beta-amyloid precursor protein ectodomain APPs alpha is sufficient to rescue the anatomical, behavioral, and electrophysiological abnormalities of APP-deficient mice. *J. Neurosci.* **2007**, *27* (29), 7817−7826.

(17) Ho, A.; Liu, X.; Sudhof, T. C. Deletion of Mint proteins decreases amyloid production in transgenic mouse models of Alzheimer's disease. *J. Neurosci.* **2008**, *28* (53), 14392−14400.

(18) Lau, K. F.; McLoughlin, D. M.; Standen, C.; Miller, C. C. X11 alpha and x11 beta interact with presenilin-1 via their PDZ domains. *Mol. Cell. Neurosci.* **2000**, *16* (5), 557−565.

(19) Biederer, T.; Cao, X.; Sudhof, T. C.; Liu, X. Regulation of APP-dependent transcription complexes by Mint/X11s: differential functions of Mint isoforms. *J. Neurosci.* **2002**, *22* (17), 7340−7351.

(20) Xie, Z.; Romano, D. M.; Tanzi, R. E. RNA interference-mediated silencing of X11alpha and X11beta attenuates amyloid beta-protein levels via differential effects on beta-amyloid precursor protein processing. *J. Biol. Chem.* **2005**, *280* (15), 15413−15421.

(21) Sullivan, S. E.; Dillon, G. M.; Sullivan, J. M.; Ho, A. Mint proteins are required for synaptic activity-dependent amyloid precursor protein (APP) trafficking and amyloid beta generation. *J. Biol. Chem.* **2014**, *289* (22), 15374−15383.

(22) McLoughlin, D. M.; Irving, N. G.; Brownlees, J.; Brion, J. P.; Leroy, K.; Miller, C. C. Mint2/X11-like colocalizes with the Alzheimer's disease amyloid precursor protein and is associated with neuritic plaques in Alzheimer's disease. *Eur. J. Neurosci* **1999**, *11* (6), 1988−1994.

(23) Jacobs, E. H.; Williams, R. J.; Francis, P. T. Cyclin-dependent kinase 5, Munc18a and Munc18-interacting protein 1/X11alpha protein up-regulation in Alzheimer's disease. *Neuroscience* **2006**, *138* (2), 511−522.

(24) Lee, J. H.; Lau, K. F.; Perkinton, M. S.; Standen, C. L.; Shemilt, S. J.; Mercken, L.; Cooper, J. D.; McLoughlin, D. M.; Miller, C. C. The neuronal adaptor protein X11alpha reduces Abeta levels in the brains of Alzheimer's APPswe Tg2576 transgenic mice. *J. Biol. Chem.* **2003**, *278* (47), 47025−47029.

(25) Lee, J. H.; Lau, K. F.; Perkinton, M. S.; Standen, C. L.; Rogelj, B.; Falinska, A.; McLoughlin, D. M.; Miller, C. C. The neuronal adaptor protein X11beta reduces amyloid beta-protein levels and amyloid plaque formation in the brains of transgenic mice. *J. Biol. Chem.* **2004**, *279* (47), 49099−49104.

(26) Sano, Y.; Syuzo-Takabatake, A.; Nakaya, T.; Saito, Y.; Tomita, S.; Itohara, S.; Suzuki, T. Enhanced amyloidogenic metabolism of the amyloid beta-protein precursor in the X11L-deficient mouse brain. *J. Biol. Chem.* **2006**, *281* (49), 37853−37860.

(27) Saito, Y.; Sano, Y.; Vassar, R.; Gandy, S.; Nakaya, T.; Yamamoto, T.; Suzuki, T. X11 proteins regulate the translocation of amyloid beta-protein precursor (APP) into detergent-resistant membrane and suppress the amyloidogenic cleavage of APP by beta-site-cleaving enzyme in brain. *J. Biol. Chem.* **2008**, *283* (51), 35763−35771.

(28) Saluja, I.; Paulson, H.; Gupta, A.; Turner, R. S. X11alpha haploinsufficiency enhances Abeta amyloid deposition in Alzheimer's disease transgenic mice. *Neurobiol. Dis.* **2009**, *36* (1), 162−168.

(29) Mitchell, J. C.; Ariff, B. B.; Yates, D. M.; Lau, K. F.; Perkinton, M. S.; Rogelj, B.; Stephenson, J. D.; Miller, C. C.; McLoughlin, D. M. X11beta rescues memory and long-term potentiation deficits in Alzheimer's disease APPswe Tg2576 mice. *Hum. Mol. Genet.* **2009**, *18* (23), 4492−4500.

(30) Kondo, M.; Shiono, M.; Itoh, G.; Takei, N.; Matsushima, T.; Maeda, M.; Taru, H.; Hata, S.; Yamamoto, T.; Saito, Y.; Suzuki, T. Increased amyloidogenic processing of transgenic human APP in X11-like deficient mouse brain. *Mol. Neurodegener.* **2010**, *5*, 35.

(31) Uhlik, M. T.; Temple, B.; Bencharit, S.; Kimple, A. J.; Siderovski, D. P.; Johnson, G. L. Structural and evolutionary division of phosphotyrosine binding (PTB) domains. *J. Mol. Biol.* **2005**, *345* (1), 1−20.

(32) Matos, M. F.; Xu, Y.; Dulubova, I.; Otwinowski, Z.; Richardson, J. M.; Tomchick, D. R.; Rizo, J.; Ho, A. Autoinhibition of Mint1 adaptor protein regulates amyloid precursor protein binding and processing. *Proc. Natl. Acad. Sci. U. S. A.* **2012**, *109* (10), 3802−3807.

(33) Valiyaveetil, F. I.; Sekedat, M.; MacKinnon, R.; Muir, T. W. Structural and functional consequences of an amide-to-ester substitution in the selectivity filter of a potassium channel. *J. Am. Chem. Soc.* **2006**, *128* (35), 11591−11599.
(34) Eildal, J. N.; Hultqvist, G.; Balle, T.; Stuhr-Hansen, N.; Padrah, S.; Gianni, S.; Stromgaard, K.; Jemth, P. Probing the role of backbone hydrogen bonds in protein-peptide interactions by amide-to-ester mutations. *J. Am. Chem. Soc.* **2013**, *135* (35), 12998−13007.
(35) Pedersen, S. W.; Pedersen, S. B.; Anker, L.; Hultqvist, G.; Kristensen, A. S.; Jemth, P.; Stromgaard, K. Probing backbone hydrogen bonding in PDZ/ligand interactions by protein amide-to-ester mutations. *Nat. Commun.* **2014**, *5*, 3215.
(36) Pedersen, S. W.; Hultqvist, G.; Stromgaard, K.; Jemth, P. The role of backbone hydrogen bonds in the transition state for protein folding of a PDZ. domain. *PLoS One* **2014**, *9* (4), e95619.
(37) Lynagh, T.; Flood, E.; Boiteux, C.; Wulf, M.; Komnatnyy, V. V.; Colding, J. M.; Allen, T. W.; Pless, S. A. A selectivity filter at the intracellular end of the acid-sensing ion channel pore. *eLife* **2017**, *6*, e24630.
(38) Deechongkit, S.; Dawson, P. E.; Kelly, J. W. Toward assessing the position-dependent contributions of backbone hydrogen bonding to beta-sheet folding thermodynamics employing amide-to-ester perturbations. *J. Am. Chem. Soc.* **2004**, *126* (51), 16762−16771.
(39) Deechongkit, S.; You, S. L.; Kelly, J. W. Synthesis of all nineteen appropriately protected chiral alpha-hydroxy acid equivalents of the alpha-amino acids for Boc solid-phase depsi-peptide synthesis. *Org. Lett.* **2004**, *6* (4), 497−500.
(40) Stuhr-Hansen, N.; Padrah, S.; Strømgaard, K. Facile synthesis of α-hydroxy carboxylic acids from the corresponding α-amino acids. *Tetrahedron Lett.* **2014**, *55* (30), 4149−4151.
(41) Powers, E. T.; Deechongkit, S.; Kelly, J. W. Backbone-Backbone H-Bonds Make Context-Dependent Contributions to Protein Folding Kinetics and Thermodynamics: Lessons from Amide-to-Ester Mutations. *Adv. Protein Chem.* **2005**, *72*, 39−78.
(42) Deechongkit, S.; Nguyen, H.; Powers, E. T.; Dawson, P. E.; Gruebele, M.; Kelly, J. W. Context-dependent contributions of backbone hydrogen bonding to beta-sheet folding energetics. *Nature* **2004**, *430* (6995), 101−105.
(43) Bieschke, J.; Siegel, S. J.; Fu, Y.; Kelly, J. W. Alzheimer's Abeta peptides containing an isostructural backbone mutation afford distinct aggregate morphologies but analogous cytotoxicity. Evidence for a common low-abundance toxic structure(s)? *Biochemistry* **2008**, *47* (1), 50−59.
(44) Bunagan, M. R.; Gao, J.; Kelly, J. W.; Gai, F. Probing the folding transition state structure of the villin headpiece subdomain via side chain and backbone mutagenesis. *J. Am. Chem. Soc.* **2009**, *131* (21), 7470−7476.
(45) Yajnik, V.; Blaikie, P.; Bork, P.; Margolis, B. Identification of residues within the SHC phosphotyrosine binding/phosphotyrosine interaction domain crucial for phosphopeptide interaction. *J. Biol. Chem.* **1996**, *271* (4), 1813−1816.
(46) Smith, M. J.; Hardy, W. R.; Murphy, J. M.; Jones, N.; Pawson, T. Screening for PTB domain binding partners and ligand specificity using proteome-derived NPXY peptide arrays. *Mol. Cell. Biol.* **2006**, *26* (22), 8461−8474.
(47) Taylor, J. W. The synthesis and study of side-chain lactam-bridged peptides. *Biopolymers* **2002**, *66* (1), 49−75.
(48) Bach, A.; Chi, C. N.; Olsen, T. B.; Pedersen, S. W.; Roder, M. U.; Pang, G. F.; Clausen, R. P.; Jemth, P.; Stromgaard, K. Modified peptides as potent inhibitors of the postsynaptic density-95/N-methyl-D-aspartate receptor interaction. *J. Med. Chem.* **2008**, *51* (20), 6450−6459.
(49) Wender, P. A.; Mitchell, D. J.; Pattabiraman, K.; Pelkey, E. T.; Steinman, L.; Rothbard, J. B. The design, synthesis, and evaluation of molecules that enable or enhance cellular uptake: peptoid molecular transporters. *Proc. Natl. Acad. Sci. U. S. A.* **2000**, *97* (24), 13003−13008.
(50) Hill, M. D.; Goyal, M.; Menon, B. K.; Nogueira, R. G.; McTaggart, R. A.; Demchuk, A. M.; Poppe, A. Y.; Buck, B. H.; Field, T. S.; Dowlatshahi, D.; van Adel, B. A.; Swartz, R. H.; Shah, R. A.; Sauvageau, E.; Zerna, C.; Ospel, J. M.; Joshi, M.; Almekhlafi, M. A.; Ryckborst, K. J.; Lowerison, M. W.; Heard, K.; Garman, D.; Haussen, D.; Cutting, S. M.; Coutts, S. B.; Roy, D.; Rempel, J. L.; Rohr, A. C.; Iancu, D.; Sahlas, D. J.; Yu, A. Y. X.; Devlin, T. G.; Hanel, R. A.; Puetz, V.; Silver, F. L.; Campbell, B. C. V.; Chapot, R.; Teitelbaum, J.; Mandzia, J. L.; Kleinig, T. J.; Turkel-Parrella, D.; Heck, D.; Kelly, M. E.; Bharatha, A.; Bang, O. Y.; Jadhav, A.; Gupta, R.; Frei, D. F.; Tarpley, J. W.; McDougall, C. G.; Holmin, S.; Rha, J. H.; Puri, A. S.; Camden, M. C.; Thomalla, G.; Choe, H.; Phillips, S. J.; Schindler, J. L.; Thornton, J.; Nagel, S.; Heo, J. H.; Sohn, S. I.; Psychogios, M. N.; Budzik, R. F.; Starkman, S.; Martin, C. O.; Burns, P. A.; Murphy, S.; Lopez, G. A.; English, J.; Tymianski, M.; Investigators, E.-N. Efficacy and safety of nerinetide for the treatment of acute ischaemic stroke (ESCAPE-NA1): a multicentre, double-blind, randomised controlled trial. *Lancet* **2020**, *395* (10227), 878−887.
(51) Dovey, H. F.; John, V.; Anderson, J. P.; Chen, L. Z.; de Saint Andrieu, P.; Fang, L. Y.; Freedman, S. B.; Folmer, B.; Goldbach, E.; Holsztynska, E. J.; Hu, K. L.; Johnson-Wood, K. L.; Kennedy, S. L.; Kholodenko, D.; Knops, J. E.; Latimer, L. H.; Lee, M.; Liao, Z.; Lieberburg, I. M.; Motter, R. N.; Mutter, L. C.; Nietz, J.; Quinn, K. P.; Sacchi, K. L.; Seubert, P. A.; Shopp, G. M.; Thorsett, E. D.; Tung, J. S.; Wu, J.; Yang, S.; Yin, C. T.; Schenk, D. B.; May, P. C.; Altstiel, L. D.; Bender, M. H.; Boggs, L. N.; Britton, T. C.; Clemens, J. C.; Czilli, D. L.; Dieckman-McGinty, D. K.; Droste, J. J.; Fuson, K. S.; Gitter, B. D.; Hyslop, P. A.; Johnstone, E. M.; Li, W. Y.; Little, S. P.; Mabry, T. E.; Miller, F. D.; Audia, J. E. Functional gamma-secretase inhibitors reduce beta-amyloid peptide levels in brain. *J. Neurochem.* **2001**, *76* (1), 173−181.
(52) Tunnemann, G.; Ter-Avetisyan, G.; Martin, R. M.; Stockl, M.; Herrmann, A.; Cardoso, M. C. Live-cell analysis of cell penetration ability and toxicity of oligo-arginines. *J. Pept. Sci.* **2008**, *14* (4), 469−476.
(53) Rousselle, C.; Clair, P.; Smirnova, M.; Kolesnikov, Y.; Pasternak, G. W.; Gac-Breton, S.; Rees, A. R.; Scherrmann, J. M.; Temsamani, J. Improved brain uptake and pharmacological activity of dalargin using a peptide-vector-mediated strategy. *J. Pharmacol. Exp. Ther.* **2003**, *306* (1), 371−376.
(54) Oller-Salvia, B.; Sanchez-Navarro, M.; Ciudad, S.; Guiu, M.; Arranz-Gibert, P.; Garcia, C.; Gomis, R. R.; Cecchelli, R.; Garcia, J.; Giralt, E.; Teixido, M. MiniAp-4: A Venom-Inspired Peptidomimetic for Brain Delivery. *Angew. Chem., Int. Ed.* **2016**, *55* (2), 572−575.
(55) Miller, C. C.; McLoughlin, D. M.; Lau, K. F.; Tennant, M. E.; Rogelj, B. The X11 proteins, Abeta production and Alzheimer's disease. *Trends Neurosci.* **2006**, *29* (5), 280−285.
(56) Das, U.; Scott, D. A.; Ganguly, A.; Koo, E. H.; Tang, Y.; Roy, S. Activity-induced convergence of APP and BACE-1 in acidic microdomains via an endocytosis-dependent pathway. *Neuron* **2013**, *79* (3), 447−460.
(57) Das, U.; Wang, L.; Ganguly, A.; Saikia, J. M.; Wagner, S. L.; Koo, E. H.; Roy, S. Visualizing APP and BACE-1 approximation in neurons yields insight into the amyloidogenic pathway. *Nat. Neurosci.* **2016**, *19* (1), 55−64.
(58) O'Brien, R. J.; Wong, P. C. Amyloid precursor protein processing and Alzheimer's disease. *Annu. Rev. Neurosci.* **2011**, *34*, 185−204.

https://dx.doi.org/10.1021/jacs.0c10696
J. Am. Chem. Soc. 2021, 143, 891−901